EFFICIENT SIMULATION OF ACOUSTIC PHYSICAL MODELS WITH NONLINEAR DISSIPATION

Riccardo Russo
Department of
Industrial Engineering
University of Bologna
Bologna, Italy
riccardo.russo19@unibo.it

Michele Ducceschi
Department of
Industrial Engineering
University of Bologna
Bologna, Italy

Stefan Bilbao
Acoustics & Audio Group
University of Edinburgh
Edinburgh, UK

Matthew Hamilton
Department of
Industrial Engineering
University of Bologna
Bologna, Italy

ABSTRACT

One long-term goal of physics-based sound synthesis and audio effect modeling has been to open the door to models without a counterpart in the real world. Less explored has been the fine-grained adjustment of the constituent physical laws that underpin such models. In this paper, the introduction of a nonlinear damping law into a plate reverberation model is explored, through the use of four different functions, transferred from the setting of virtual-analog electronics. First, a case study of an oscillator with nonlinear damping is investigated. Results are compared against linear dissipation, illustrating differing spectral characteristics. To solve the systems, a recently proposed numerical solver is employed, that entirely avoids the use of iterative routines such as Newton-Raphson for solving nonlinearities, thus allowing very efficient numerical solution. This scheme is then used to simulate a plate reverbation unit, and tests are run, to investigate spectral variations induced by nonlinear damping. Finally, a musical case is presented that includes frequency-dependent damping coefficients.

1. INTRODUCTION

In recent years, physical modelling-based techniques gained importance in the field of sound synthesis [1], and different methods were developed over time [2–4].

Despite allowing to synthesize natural and realistic sounds, the main drawback of physical modelling synthesis lies in the computational cost required by the simulation algorithms, which is much larger with respect to other synthesis techniques [1]. This is particularly true when dealing with nonlinearities, which are of critical importance in sound synthesis. In particular, virtual-analog models, which emulate analog electroacoustical devices, often need to include of nonlinear components such as diodes [5]. In order to guarantee a passive energy balance of the discrete numerical schemes, the simulation algorithms mostly rely on fully-implicit methods [5, 6], which require the use of iterative routines such as Newton-Raphson to be solved. These methods are computationally expensive and serial in nature, requiring to iterate multiple times per time-step to converge to a solution. Other issues emerge, such as a variable computational cost per time-step, linked to the number of iterations, and the necessity to choose appropriate tolerance thresholds and iterations caps. In addition, existence and uniqueness of the computed solutions is generally not ensured [7]. A numerical method was recently proposed [8, 9], which allows for the solution of ordinary differential equations (ODEs) by employing a linearly-implicit time-stepping procedure. This way, the system is updated by simply solving one linear system, thus avoiding the use of iterative routines. This method was successfully employed for the simulation of virtual-analog [9] and acoustical systems [10].

One long-term goal of physical modelling sound synthesis and virtual-analog modeling has been to open the door to models without a counterpart in the real world. In particular, less explored has been the fine-grained adjustment of the constituent physical laws that underpin such models. In this work, the introduction of nonlinear damping into an electroacoustical unit, such as a plate reverb, is explored. In the context of virtual-analog, Bilbao et al. were among the firsts to develop a physical model of a plate reverb, making use of FDTD techniques [11]. Later, Ducceschi and Webb [12] employed a modal approach for developing a plugin simulating the EMT 140 plate reverb. Commercial plug-ins based on physical modelling are also available, see e.g. Physical Audio [1] and UVI [2]. In this paper, the plate is simulated with the modal approach seen in [12], while the damping functions employed are those typically found in virtual-analog models, as they are naturally expressed as energy dissipation functions inside circuits. Finally, the non iterative method [9] is employed as a time-stepping scheme, to ensure efficiency.

The paper is structured as follows: Section 2 presents the case study of a damped, forced oscillator. Here, the four damping functions are illustrated, and a test compares the nonlinear systems outputs with the response of a linearly damped oscillator. In section 3 a plate model is developed, and a test investigates the differences introduced by nonlinear damping. In section 4 the case of a plate with frequency-dependent damping coefficients is presented, and section 5 concludes the paper. Sound samples and higher-

[1] physicalaudio.co.uk/products/dynamic-plate-reverb
[2] www.uvi.net/plate.html

resolution images are available on GitHub [3].

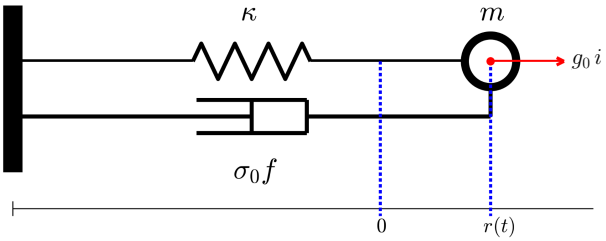

Figure 1: Damped mass-spring system with forcing. The system frequency can be defined by means of the mass m and the spring stiffness κ with the relation: $\omega_0 = \sqrt{\kappa/m}$.

2. CASE STUDY: SIMPLE HARMONIC OSCILLATOR

It is convenient to start by considering a simple dynamical system with a single degree of freedom (DOF): a mass-spring system with an added nonlinear damping mechanism, driven by an input signal. The system can be described by the equation:

$$\ddot{r} = -\omega_0^2 r - \sigma_0 f(\eta) + g_0\, i, \quad \eta = a\dot{r}, \tag{1}$$

which is a second-order ODE in time. Here, $r = r(t) : \mathbb{R}_0^+ \to \mathbb{R}$ represents the displacement of the mass, in meters, from the equilibrium position, which depends on time $t \geq 0$; ω_0 is the angular frequency of the oscillator in rad/s, and is defined as: $\omega_0 = \sqrt{\kappa/m}$, where κ is the spring stiffness, and m is the oscillator mass in Kg. The function $i = i(t)$ is a normalized, dimensionless forcing signal, multiplied by an amplification factor $g_0 \in \mathbb{R}_0^+$, with dimension N/Kg, and $f(\eta) : \mathbb{R} \to \mathbb{R}$ is a general nonlinear function, depending on the oscillator velocity $\dot{r}$. The damping is parameterized by two real constants $\sigma_0 > 0$, $a > 0$: the first sets the amount of damping of the system, and has dimension of Kg^{-1}, while the latter is a free, dimensionless parameter. In this paper, it is assumed that f satisfies the following conditions:

$$\eta\, f(\eta) \geq 0 \tag{2a}$$

$$\lim_{|\eta|\to 0} f(\eta)/\eta < \infty\,. \tag{2b}$$

Property (2a) is referred to as sector-boundedness [9], here to sector $[0, \infty]$, while condition (2b) enforces boundedness of f/x at the origin. Both properties (2) are essential for the non-iterative method described in [9].

2.1 Energy Balance

An energy balance for this system can be obtained by multiplying equation (1) by $\dot{r}$. One then gets [4]:

$$\frac{d}{dt}\underbrace{\left(\frac{\dot{r}^2}{2} + \frac{\omega_0^2 r^2}{2}\right)}_{H} = -\dot{r}\,\sigma_0\, f(\eta) + \dot{r}\, g_0\, i, \tag{3}$$

[3] github.com/Nemus-Project/plate-saturator

where H is the system energy, scaled by the mass, and the input term has now dimension of a power, again divided by a mass. Therefore:

$$\dot{H} = -\,\sigma_0\, \eta f(\eta)/a + \dot{r}\, g_0\, i. \tag{4}$$

Owing to condition (2a), and to the non negativity of σ_0 and a one obtains, in the zero-input case:

$$\dot{H} \leq 0; \tag{5}$$

which is the condition for passivity.

2.2 First-Order Form

The non-iterative method described in [9] applies to first-order ODEs. Therefore, it is necessary to express equation (1) in first-order form. To this end, one may define a generalized coordinate q and a momentum p such that:

$$q \triangleq \omega_0 r; \quad p \triangleq \dot{r}, \tag{6}$$

with p being the momentum normalized by the mass. Thus, the system energy takes the form:

$$H = p^2/2 + q^2/2. \tag{7}$$

Equation (1) can then be re-written as:

$$\dot{\mathbf{x}} = \mathbf{J}\nabla H - \mathbf{c} f(\eta) + \boldsymbol{\xi} i. \tag{8}$$

Here:

$$\mathbf{x} = \begin{bmatrix} q \\ p \end{bmatrix}, \; \mathbf{J} = \begin{bmatrix} 0 & \omega_0 \\ -\omega_0 & 0 \end{bmatrix}, \; \mathbf{c} = \begin{bmatrix} 0 \\ \sigma_0 \end{bmatrix}, \boldsymbol{\xi} = \begin{bmatrix} 0 \\ g_0 \end{bmatrix} \tag{9}$$

and

$$\eta = \boldsymbol{\alpha}^\intercal \mathbf{x}, \quad \boldsymbol{\alpha}^\intercal = \begin{bmatrix} 0 & a \end{bmatrix}. \tag{10}$$

The gradient operator is $\nabla = [\partial/\partial q, \partial/\partial p]^\intercal$, therefore:

$$\nabla H = \mathbf{x}. \tag{11}$$

An energy balance can be obtained by left-multiplying equation (8) by $(\nabla H)^\intercal$:

$$(\nabla H)^\intercal \dot{\mathbf{x}} = (\nabla H)^\intercal \mathbf{J} \nabla H - (\nabla H)^\intercal (\mathbf{c} f(\eta) + \boldsymbol{\xi} i). \tag{12}$$

Because $\mathbf{J}$ is skew-symmetric, the first term on the right-hand side vanishes, and, owing to the chain rule, $\dot{H} = (\nabla H)^\intercal \dot{\mathbf{x}}$. Therefore, in the zero-input case:

$$\dot{H} = -\sigma_0\, p\, f(\eta) = -\sigma_0 \eta f(\eta)/a, \tag{13}$$

which is the same result obtained in (4); thus, the system dissipates. Notice that equation (8) has the form of a Port-Hamiltonian system [13–15], including energy storage and dissipation elements.

2.3 Finite Difference Operators

In the next subsections, the numerical method described in [8, 9] will be employed to numerically integrate equation (8) in time. To this end, it is first necessary to define a constant time-step k, yielding a sampling rate: $f_s = 1/k$.

A continuous function $r(t)$ may be approximated by a discrete time series r^n at time instants $t_n = kn$, where $n \in \mathbb{N}$ is the time index.

With a time-grid defined, it is possible to write the basic identity and shift operators:

$$1r^n = r^n, \quad e_+ r^n = r^{n+1}, \quad e_- r^n = r^{n-1}. \tag{14}$$

The latter are used to write the time-difference operators:

$$\delta_+ = (e_+ - 1)/k, \quad \delta_- = (1 - e_-)/k. \tag{15}$$

These are the forward and backward operators respectively. Finally, averaging operators can be written as:

$$\mu_+ = (e_+ + 1)/2, \ \mu_- = (1 + e_-)/2. \tag{16}$$

2.4 Non-Iterative Numerical Scheme

It is now possible to adapt the solver proposed by Ducceschi et al. [9] to numerically integrate equation (8) in time, in a similar fashion to what seen in [10]. A numerical scheme is given as follows:

$$\begin{cases} \boldsymbol{\sigma}^{(P)} \delta_+ \mathbf{x}^n = \mathbf{J} \nabla \mathfrak{h}^{n+1/2} - \mathbf{c} d^n \mu_+ \eta^n + \boldsymbol{\xi} \mu_+ i^n \\ \eta^n = \boldsymbol{\alpha}^\intercal \mathbf{x}^n, \end{cases} \tag{17}$$

where the discrete energy is:

$$\mathfrak{h}(q^n, p^n) \triangleq \mathfrak{h}^n = (p^n)^2/2 + (q^n)^2/2. \tag{18}$$

In order to compute the gradient, consider the discrete partial derivative of $\mathfrak{h}$ with respect to q:

$$\delta_{q+} \mathfrak{h}(q^n, p^n) = \frac{\mathfrak{h}(q^{n+1}, p^n) - \mathfrak{h}(q^n, p^n)}{q^{n+1} - q^n} = \mu_+ q^n. \tag{19}$$

An analogous result holds for p; therefore:

$$\nabla \mathfrak{h}^{n+1/2} \triangleq [\delta_{q+} \mathfrak{h}^n, \delta_{p+} \mathfrak{h}^n]^\intercal = \mu_+ \mathbf{x}^n. \tag{20}$$

Notice that, because the forward average operator computes the mean between two samples at time instants n and $n+1$, the discrete energy gradient in 20 is defined on an interleaved time-grid.

In equation (17), $\boldsymbol{\sigma}^{(P)} = \boldsymbol{\sigma}^{(P)}(\mathbf{x}^n)$ is a factor taking the form of a perturbation expansion, which can be set to yield a truncation error with an accuracy of order $(P+1)$. Following [9], its expression is:

$$\boldsymbol{\sigma}^{(P)}(\mathbf{x}^n) = \sum_{p=0}^{P} k^p \boldsymbol{\zeta}^{(p)}(\mathbf{x}^n). \tag{21}$$

The functions $\boldsymbol{\zeta}^{(p)}(\mathbf{x}^n)$ are obtained by means of technique which has strong links to the modified equation method [16]. The first two terms are here given explicitly as:

$$\boldsymbol{\zeta}^{(0)}(\mathbf{x}^n) = \mathbf{I} \tag{22a}$$

$$\boldsymbol{\zeta}^{(1)}(\mathbf{x}^n) = \mathbf{c}\boldsymbol{\alpha}^\intercal (\lambda^n - d^n)/2. \tag{22b}$$

where

$$\lambda^n \triangleq df/d\eta\big|_{\eta=\eta^n}, \quad d^n \triangleq f/\eta\big|_{\eta=\eta^n}. \tag{23}$$

Thus, with $P = 1$ one gets a factor:

$$\boldsymbol{\sigma}^{(1)}(\mathbf{x}^n) = \mathbf{I} + k\mathbf{c}\boldsymbol{\alpha}^\intercal (\lambda^n - d^n)/2, \tag{24}$$

which allows the formulation of a second-order accurate numerical scheme. A proof of this is obtained easily by applying scheme (17) to the continuous function $\mathbf{x}(t)$, assumed to solve the continuous equation (8). Taylor-expanding around $t_n := kn$, one obtains a truncation error going as $\mathcal{O}(k^2)$.

Expanding the operators in equation (17) yields the update:

$$\mathbf{A}^n \mathbf{x}^{n+1} = \mathbf{B}^n \mathbf{x}^n + k\boldsymbol{\xi}\mu_+ i^n, \tag{25}$$

with:

$$\begin{aligned} \mathbf{A}^n &= \mathbf{I} + k\,\mathbf{c}\boldsymbol{\alpha}^\intercal \lambda^n/2 - k\,\mathbf{J}/2 \\ \mathbf{B}^n &= \mathbf{I} + k\,\mathbf{c}\boldsymbol{\alpha}^\intercal (\lambda^n - 2d^n)/2 + k\,\mathbf{J}/2. \end{aligned} \tag{26}$$

Notice that both $\mathbf{A}^n$ and $\mathbf{B}^n$ only include values at time-step n; therefore, the state at $n+1$ can be computed with a single 2×2 matrix inversion, without relying on iterative routines. Furthermore, the oscillator position in meters r^n can be retrieved at each time sample with: $r^n = q^n/\omega_0$.

Regarding passivity of scheme (17), a discrete version of the energy balance (4) is not directly available; nevertheless, partial results on the stability properties of these kind of solvers are available in [9].

2.5 Nonlinear Dissipation

The numerical scheme presented above holds for any function $f(\eta)$, provided that it satisfies properties (2). Here, four different expressions for nonlinear dissipation are given, all borrowed from the virtual-analog world. These are: the cubic nonlinearity, which is the first nonlinear polynomial term satisfying properties (2); the hyperbolic tangent, used as a soft-clipping mechanism, for instance in the Moog ladder filter [17]; the hyperbolic sine, found into diode clipper models [18]; and the exponential nonlinearity, from the Shockley diode model. Table 1 reports the expressions for $f(\eta)$, along with the components for d and λ.

	Cubic	Tanh	Sinh	Exp
$f(\eta)$	$\eta + \eta^3$	$\tanh(\eta)$	$\sinh(\eta)$	$e^\eta - 1$
$d(\eta)$	$1 + \eta^2$	$\tanh(\eta)/\eta$	$\sinh(\eta)/\eta$	$(e^\eta - 1)/\eta$
$\lambda(\eta)$	$1 + 3\eta^2$	$\mathrm{sech}^2(\eta)$	$\cosh(\eta)$	e^η

Table 1: Nonlinear dissipation functions $f(\eta)$ and associated d and λ expressions.

Finally, it is convenient to define a scheme with a more "classic" linear viscous friction. This system will be used as a reference, and the solution will be compared against the outputs of the nonlinear systems, in order to investigate the differences introduced by nonlinear dissipation. One sets $f^n = \eta^n$; therefore, $d^n = \lambda^n = 1$ and scheme (17) reduces to:

$$\delta_+ \mathbf{x}^n = \mathbf{J} \nabla \mathfrak{h}^{n+1/2} - \mathbf{c}\mu_+ \eta^n + \boldsymbol{\xi}\mu_+ i^n, \tag{27}$$

which is equivalent to the midpoint method [16] applied to a damped simple harmonic oscillator.

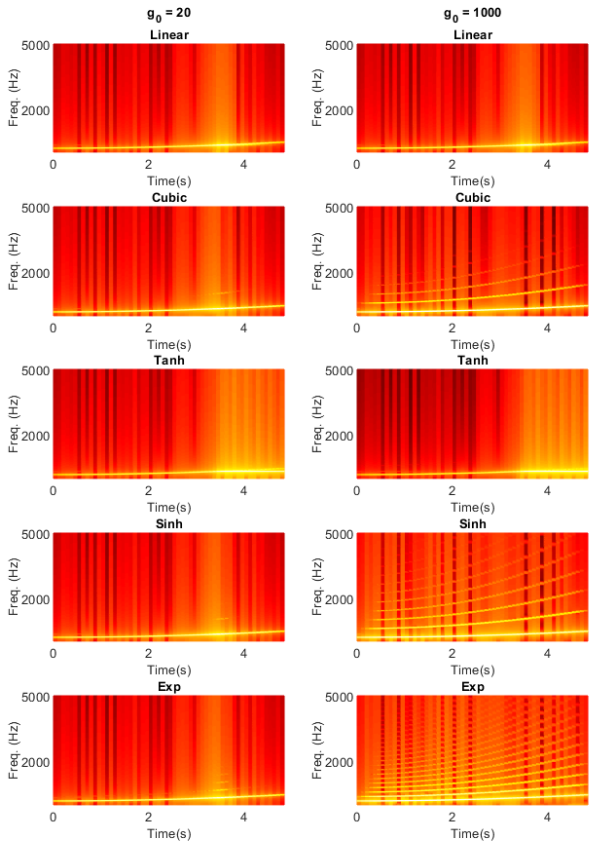

Figure 2: Outputs of the five oscillators, driven with sine sweeps, under two different values of gain g.

2.6 Numerical Experiments

Figure 2 displays the outputs of the five oscillators, driven with a quadratic sine sweep, ranging from 200 to 500 Hz, under two different values for the gain g. The sample rate was $f_s = 2 \cdot 44100$ Hz; the oscillator angular frequency was set to $\omega_0 = 350 \cdot 2 \cdot \pi$ rad/s, falling into the input signal frequency range, and the parameters σ_0 and a were 1 and 20 respectively. Output samples were normalized between $[-1, 1]$, in order to better observe differences in the spectral contents.

As expected, the linear system output does not depend on input amplitude variations. On the other hand, the "cubic", "sinh" and "exp" nonlinearities produce an enrichment in the frequency spectrum, as the gain increases. Notice that the "sinh" and "cubic" systems only produce odd harmonics: this makes sense, since the hyperbolic sine and the cubic only include odd terms in their Taylor expansion. The exponential expansion instead presents even and odd terms; as a result, the "exp" spectrum includes even harmonics as well. The "tanh" nonlinearity presents a completely different behaviour. The function itself is nearly linear around the origin, and almost constant for greater values of η, where it can be approximated by zero-order polynomials of values -1 and 1. Therefore, there is no creation of spectral content; furthermore, this produces a constant, low damping for all frequencies, contrary to linear damping, where friction increases linearly with speed.

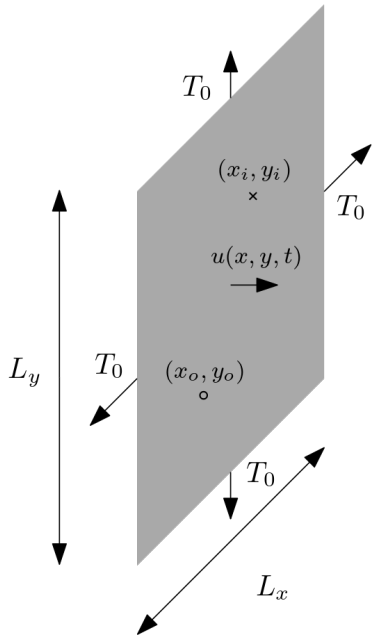

Figure 3: Geometrical scheme of a thin rectangular plate.

3. PLATE MODEL

A plate reverb can be described by a flat, rectangular plate, as represented in Figure 3. In the hypothesis of small vibrations, this system is described by the Kirchhoff equation, here given with a forcing term, and no damping:

$$\rho H \frac{\partial^2 u}{\partial t^2} = T_0 \nabla^2 u - D \nabla^4 u + \delta(x - x_i)\delta(y - y_i) g i. \quad (28)$$

Here, $u = u(x, y, t)$ represents the transverse displacement, ∇ is the gradient operator, and the plate occupies a region $\mathcal{D} = [0, L_x] \times [0, L_y]$. Notice that model (28) holds under the condition $H \ll L_x, L_y$, where H is the plate thickness. The other constants are: volumetric density ρ, tension T_0; D is the fexural rigidity, and is expressed as: $D = Eh^3/[12(1 - \nu^2)]$, where E is Young's modulus and ν is Poisson's ratio. The function $i = i(t)$ represents the normalized, dimensionless driving signal, with gain g, coordinates x_i, y_i indicate the input location on the plate and the Dirac deltas specify point-wise forcing. Notice that, in this case, g has dimension of a force.

In this work, a modal approach is employed to solve equation (28), following Ducceschi and Webb [12]. To this end, the solution u is expressed as a superposition of modal displacements $\Phi_m(x, y)$ and time evolutions $r_m(t)$:

$$u = \sum_{m=1}^{M} \Phi_m r_m, \quad (29)$$

where M is in theory infinite, but will be limited for practical purposes. The mode shapes (eigenfunctions) must satisfy the boundary conditions. In this work, simply-

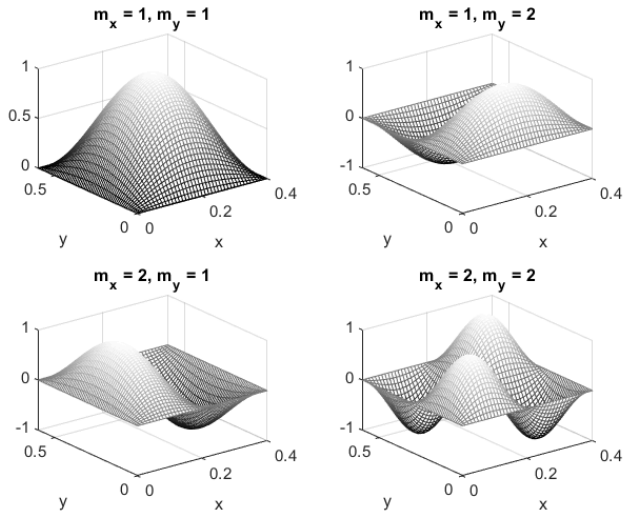

Figure 4: First four mode shapes of a rectangular plate with simply supported boundary conditions, and associated indices m_x, m_y.

supported boundaries are considered, and one has [19]:

$$\Phi_m(x,y) = \sqrt{\frac{4}{L_x L_y}} \sin\frac{m_x \pi x}{L_x} \sin\frac{m_y \pi y}{L_y}, \tag{30}$$

where m_x, m_y are a pair of integers that indicate the mode number in the x and y directions. In this paper, borrowing the notation from [12], these were merged into the single index m for easiness of notation. The first four mode shapes are depicted in Figure 4. Functions Φ_m are orthonormal under the $\mathcal{L}^2$ inner product; therefore: $\|\Phi_m\|_{\mathcal{D}} = 1$. Substituting equation (29) into (28), left-multiplying by (30) and taking an $\mathcal{L}^2$ inner product over $\mathcal{D}$ yields the equations that describe the time evolution of the modes:

$$\ddot{r}_m + \omega_m^2 r_m = g_m i, \tag{31}$$

with $g_m := \Phi_m(x_i, y_i) g/\rho H$. Here the ω_m are the eigenfrequencies of the system, which take the form:

$$\omega_m = \sqrt{\frac{T_0 \pi^2}{\rho H}\left(\frac{m_x^2}{L_x^2} + \frac{m_y^2}{L_y^2}\right) + \frac{D\pi^4}{\rho H}\left(\frac{m_x^2}{L_x^2} + \frac{m_y^2}{L_y^2}\right)^2}.$$

Finally, the displacement in meters can be retrieved at a desired position (x_o, y_o) with:

$$u(x_o, y_o) = \sum_{m=1}^{M} \Phi_m(x_o, y_o) r_m. \tag{32}$$

3.1 Including Dissipation

Equation (31) represents a system of uncoupled, undamped, forced oscillators. By including a dissipation function, one obtains an expression analogous to equation (1):

$$\ddot{r}_m = -\omega_m^2 r_m - \sigma_m f(\eta_m) + g_m i, \tag{33}$$

where $\eta_m = a_m \dot{r}_m$, and f is, as before, a generic function that satisfies properties 2.

As in Section 2, it is convenient to express equation (33) in first-order form, by defining: $q_m \triangleq \omega_m r_m$, $p_m \triangleq \dot{r}_m$. The energy for a single mode m then becomes:

$$H_m = p_m^2/2 + q_m^2/2 \tag{34}$$

Therefore, equation (33) can then be re-written as:

$$\begin{aligned} \dot{\mathbf{x}}_m &= \mathbf{J}_m \nabla_m H_m - \mathbf{c}_m f(\eta_m) + \boldsymbol{\xi}_m i \\ \eta_m &= \boldsymbol{\alpha}_m^\intercal \mathbf{x}_m. \end{aligned} \tag{35}$$

Here, analogously to what seen in Section 2, the equation components take the form:

$$\begin{aligned} \mathbf{x}_m = \begin{bmatrix} q_m \\ p_m \end{bmatrix},\ \mathbf{J}_m = \begin{bmatrix} 0 & \omega_m \\ -\omega_m & 0 \end{bmatrix}, \\ \mathbf{c}_m = \begin{bmatrix} 0 \\ \sigma_m \end{bmatrix}, \boldsymbol{\alpha} = \begin{bmatrix} 0 \\ a_m \end{bmatrix}, \boldsymbol{\xi}_m = \begin{bmatrix} 0 \\ g_m \end{bmatrix}, \end{aligned} \tag{36}$$

where σ_m and a_m are, respectively, the damping coefficient and free parameter for each mode. An energy balance is again obtained by left-multiplying equation (35) by $(\nabla H)^\intercal$. With the same considerations drawn in Section 2, in the zero-input case, one obtains a passive energy balance $\dot{H}_m = -\sigma_m f(\eta_m)\eta_m/a_m$ that holds for each mode.

3.2 Plate Simulation

Notice that, in this paper, a scalar approach for modal expansion was preferred to the matrix-based method employed in paper [10]. The reason for this is that the non-iterative solver detailed in [9] requires the function f to be a scalar. However, as seen in equation (33), each mode has an associated damping component, thus making f a vector of M elements, in a matrix-form modal expansion. On the other hand, the dissipation function is indeed a scalar if each mode is considered separately; hence, it is possible to apply the non-iterative solver to the "unrolled" modal expansion and solve each oscillator separately.

A second-order accurate, non-iterative numerical scheme solving equation (33) reads:

$$\begin{cases} \boldsymbol{\sigma}_m^{(1)} \delta_+ \mathbf{x}_m^n = \mathbf{J}_m \nabla \mathfrak{h}_m^{n+1/2} - \mathbf{c}_m d_m^n \mu_+ \eta_m^n + \boldsymbol{\xi}_m \mu_+ i^n \\ \eta_m^n = \boldsymbol{\alpha}_m^\intercal \mathbf{x}_m^n. \end{cases} \tag{37}$$

Here, the energy gradient is, again: $\mathfrak{h}_m^{n+1/2} = \mu_+ \mathbf{x}_m^n$, and $\boldsymbol{\sigma}_m^{(1)}(\mathbf{x}_m^n)$ is expressed as in equation (24), with the components now depending on the mode number m. To solve the system, it is possible to expand the operators, thus obtaining the update:

$$\mathbf{A}_m^n \mathbf{x}_m^{n+1} = \mathbf{B}_m^n \mathbf{x}_m^n + k\boldsymbol{\xi}_m \mu_+ i^n, \tag{38}$$

from which $\mathbf{x}_m^{n+1}$ is obtained after inversion of the 2×2 matrix $\mathbf{A}_m^n$. To simulate the full system, all the M oscillators must be updated in parallel, at each time step. Then, the displacement at the output position can be retrieved with the expression (32), remembering that $r_m = q_m/\omega_m$.

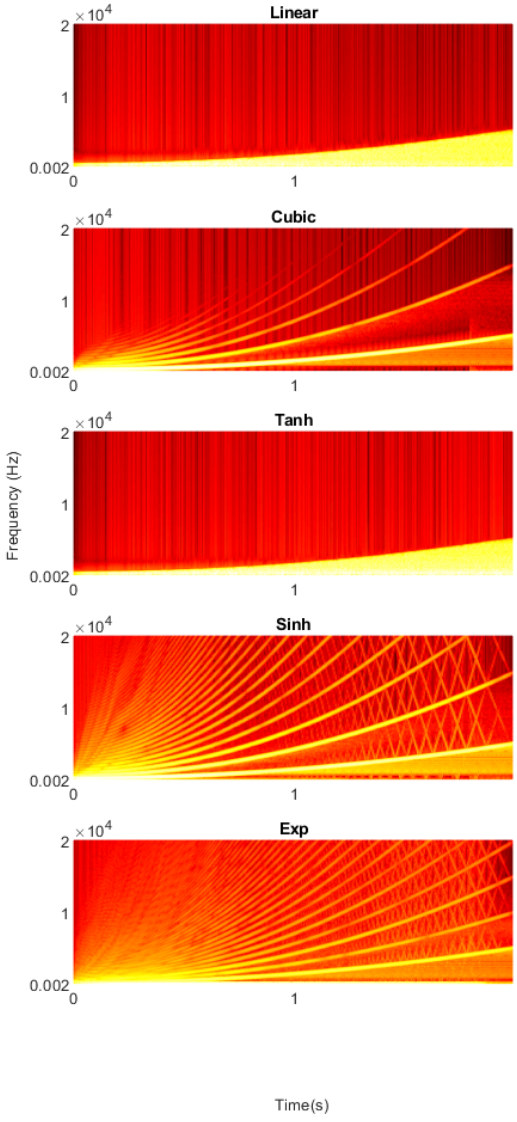

Figure 5: Outputs of the five plate models driven with sine sweeps, under a gain $g = 8000$. The high value of g, necessary for highlighting the differences in the systems responses, is responsible for the aliasing effects visible in the last two figures.

3.3 Numerical Experiments

The four nonlinear dissipation functions detailed in table 1 were again employed in scheme (38), and results were compared against linear damping, as previously done for the mass. The five systems were driven with a quadratic sine sweep, ranging from 200 to 5000 Hz, and run with a sampling rate $f_s = 2 \cdot 44100$ Hz. Parameters a and σ_0 were set to 30 and 0.1 respectively, constant for all the modes. Other constants were: $T_0 = 200$ N, $H = 0.5$ mm, $L_x = 0.4$ m, $L_y = 0.6$ m. The plate was considered to be made of steel; therefore, the physical parameters were: $\rho = 7.872 \cdot 10^3$ Kg/m^3, $E = 2 \cdot 10^{11}$ Pa and $\nu = 0.3$; these values yielded 2302 modes between 20 and 15000 Hz. Input and output positions were, respectively, $(0.52 \cdot L_x, 0.53 \cdot L_y)$ and $(0.47 \cdot L_x, 0.62 \cdot L_y)$.

A first test consisted in driving the systems with increasing gain values: it was verified that, for low-amplitude input signals, the five outputs presented no differences both in time and frequency domain; whereas for high-gain inputs it was observed a deviation from the linear behaviour. This result matches the one obtained for the mass, seen in Figure 2. Figure 5 displays the outputs of the five systems under an input gain $g = 8000$. One clearly observable difference is the increased damping introduced by the "cubic", "sinh" and "exp" nonlinearities, which are steeper than the others two: this results in higher dissipation. Moreover, as in the one-DOF case, these functions enrich the spectrum: only odd harmonics in the first two cases, both even and odd harmonics in the last one. The lower damping produced by the "tanh" nonlinearity emerges, also in this case, from the higher energy content present at the end of the spectrum.

4. A MUSICAL CASE: PHYSICAL DAMPING VALUES

Up until now, constant values for the damping coefficients σ_m were employed, in order to avoid biasing the testing; in real plates though, the amount of loss depends on the frequency. One of the advantages of the modal projection detailed in Section 4 is the possibility of setting a decay parameter for each mode. Therefore, application of refined loss profiles is immediate in this framework, unlike in time-domain approaches, where the implementation of frequency-dependent damping typically requires mixed time-space derivatives [11]. Damping in a metallic plate comes from two main sources: thermoelasticicy and radiation in the free field [20]. In addition, the EMT 140 plate reverb includes a porous panel that is used to control the decay time. The presence of the porous material modifies the impedance in the nearfield of the plate: thus, if the distance between the two elements is reduced, radiation increases. A complete model for damping is found in [21], which is based on works from Arcas [20], Cummings [22,23] and Craik [24]. Here, the damping formulae developed in [21] were employed to retrieve a set of values for some coefficients $c_m \triangleq a_m \sigma_m$, linking a_m and σ_m. Then, a value for a_m was set, constant for all the modes, and the σ_m were computed consequently. This way, increasing a_m only affects the amount of nonlinearity introduced into the system, leaving the decay rate unaffected.

Sound samples for this system are available on the GitHub companion page.

5. CONCLUSION

This work explored the introduction of nonlinear damping into a plate reverb, by making use of four functions typically employed in virtual-analog settings. It was seen that the latter affect the linear output in different manners; in particular, three of the four expressions enriched the spectral content, with responses typical of saturators. On the other hand, the Tanh nonlinearity seems to produce an output which is of less interest in musical applications. The plate was solved with a modal approach, and a recent

non-iterative numerical method was successfully applied to simulate the system. Finally, a physical model for damping was developed, and included into the model, to test the algorithm in a musical setting.

Future work will include code optimizations, and a code porting in C++, for developing a full functioning vst plugin.

Acknowledgments

This work was supported by the European Research Council (ERC), under grant 2020-StG-950084-NEMUS.

6. REFERENCES

[1] S. Bilbao, C. Desvages, M. Ducceschi, B. Hamilton, R. Harrison-Harsley, A. Torin, and C. Webb, "Physical modeling, algorithms, and sound synthesis: The ness project," *Comput. Music J.*, vol. 43, no. 2-3, pp. 15–30, 11 2020.

[2] J. Smith, "Physical modeling using digital waveguides," *Comput. Music J.*, vol. 16, p. 74, 1992.

[3] J. Adrien, "The missing link: modal synthesis," *Repres. Musical Signals*, 1991.

[4] S. Bilbao, *Numerical Sound Synthesis*. Chichester, UK: John Wiley & Sons, Ltd, 2009.

[5] R. C. D. Paiva, S. D'Angelo, J. Pakarinen, and V. Valimaki, "Emulation of operational amplifiers and diodes in audio distortion circuits," *IEEE Trans. Circuits and Systems II: Express Briefs*, vol. 59, no. 10, pp. 688–692, 2012.

[6] C. Desvages, "Physical modelling of the bowed string and applications to sound synthesis," Ph.D. dissertation, The University of Edinburgh, 2018.

[7] F. Fontana and E. Bozzo, "Newton–Raphson solution of nonlinear delay-free loop filter networks," *IEEE/ACM Trans. Audio, Speech, Lang. Process.*, vol. 27, no. 10, pp. 1590–1600, 2019.

[8] M. Ducceschi, S. Bilbao, and C. J. Webb, "Non-iterative schemes for the simulation of nonlinear audio circuits," in *Proc. Digital Audio Effects (DAFx-20in21)*, Vienna, Austria, 09 2021, pp. 25–32.

[9] M. Ducceschi and S. Bilbao, "Non-iterative simulation methods for virtual analog modelling," *IEEE/ACM Trans. Audio Speech Lang. Process.*, vol. 30, pp. 3189–3198, 2022.

[10] R. Russo, M. Ducceschi, and S. Bilbao, "Efficient simulation of the bowed string in modal form," in *Proc. Digital Audio Effects (DAFx-2022), Vienna*, Sep. 2022, pp. 122–129.

[11] S. Bilbao, K. Arcas, and A. Chaigne, "A physical model for plate reverberation," *Proc. IEEE Int. Conf. Acoust. Speech Signal Process*, vol. 5, p. 165.168, 05 2006.

[12] M. Ducceschi and C. J. Webb, "Plate reverberation: Towards the development of a real-time physical model for the working musician," in *Proc. 22nd Int. Congr. Acoust. ICA*, Buenos Aires, Argentina, 09 2016.

[13] A. van der Schaft and D. Jeltsema, "Port-hamiltonian systems theory: an introductory overview," *Found. and Trends in Syst. and Control*, vol. 1, no. 2,3, 2014.

[14] A. Falaize and T. Hélie, "Passive guaranteed simulation of analog audio circuits: a Port-Hamiltonian approach," *Appl. Sc.*, vol. 6, pp. 273 – 273, 2016.

[15] R. Müller, , and T. Hélie, "Power-balanced modelling of circuits as skew gradient systems," in *Proc. Digital Audio Effects (DAFx-19)*, Aveiro, Portugal, 09 2018.

[16] R. J. LeVeque, *Finite Difference Methods for Ordinary and Partial Differential Equations*. Philadelphia, Pennsylvania, United States: Society for Industrial and Applied Mathematics, 2007.

[17] A. Huovilainen, "Non-linear digital implementation of the moog ladder filter," in *Proc. Digital Audio Effects (DAFx-04)*, Naples, Italy, 09 2004.

[18] D. T. Yeh, J. S. Abel, A. Vladimirescu, and J. O. Smith, "Numerical methods for simulation of guitar distortion circuits," *Comput. Music J.*, vol. 32, no. 2, pp. 23–42, 2008.

[19] L. E. Kinsler, A. R. Frey, A. B. Coppens, and J. V. Sanders, *Fundamentals of Acoustics, 4th Edition*. Hoboken, NJ, USA: Wiley, 1999.

[20] K. Arcas and A. Chaigne, "On the quality of plate reverberation," *Appl. Acoust.*, vol. 71, no. 2, pp. 147–156, 2010.

[21] R. Russo, "Physical modeling and optimisation of a emt 140 plate reverb," Master's thesis, Aalborg University Copenhagen, Copenhagen, Denmark, 2021. [Online]. Available: https://projekter.aau.dk/projekter/en/studentthesis/physical-modeling-and-optimisation-of-a-emt-140-plate-reverb(3aa42a50-c36d-4f12-8adf-46ff6eeb7e7c).html

[22] A. Cummings, H. Rice, and R. Wilson, "Radiation damping in plates, induced by porous media," *J. Sound Vib.*, vol. 221, no. 1, pp. 143–167, 1999.

[23] A. Cummings, "Sound radiation from a plate into a porous medium," *J. Sound Vib.*, vol. 247, no. 3, pp. 389–406, 2001.

[24] D. Tomlinson, R. Craik, and R. Wilson, "Acoustic radiation from a plate into a porous medium," *J. Sound Vib.*, vol. 273, no. 1, pp. 33–49, 2004.